Archives of Biochemistry and Biophysics 689 (2020) 108429

Contents lists available at ScienceDirect

Archives of Biochemistry and Biophysics

journal homepage: www.elsevier.com/locate/yabbi

Biosynthesis of desferrioxamine siderophores initiated by decarboxylases: A functional investigation of two lysine/ornithine-decarboxylases from *Gordonia rubripertincta* CWB2 and *Pimelobacter simplex* 3E

Marika Hofmann[a,*], Julia S. Martin del Campo[b], Pablo Sobrado[c], Dirk Tischler[a,d,**]

[a] Environmental Microbiology, Institute of Biosciences, TU Bergakademie Freiberg, Leipziger Str. 29, 09599, Freiberg, Germany
[b] Department of Biochemistry, Virginia Tech, Blacksburg, USA
[c] Department of Biochemistry, Center Drug Discovery, Virginia Tech, Blacksburg, USA
[d] Microbial Biotechnology, Ruhr-Universität Bochum, Universitätsstr. 150, 44780, Bochum, Germany

ARTICLE INFO

Keywords:
Lysine decarboxylase
Siderophore biosynthesis
Desferrioxamines synthesis
Actinobacteria
Pyridoxal 5-phosphate cofactor

ABSTRACT

Lysine is a precursor for desferrioxamine siderophore biosynthesis. The pathway is often initiated by lysine decarboxylases. However, little is known about those enzymes from Actinobacteria which represents a diverse class of desferrioxamine producers. In this study we focused on the genes *grdesA* form *Gordonia rubripertincta* CWB2 and *psdesA* from *Pimelobacter simplex* VkMAC-2033D that encode decarboxylases presumed to be involved in the synthesis of desferrioxamine siderophores. The corresponding proteins *Gr*DesA and *Ps*DesA, were heterologously produced in *Escherichia coli* and purified. *Ps*DesA was isolated bound to the cofactor pyridoxal 5-phosphate and *Gr*DesA was purified in its apo form. *Ps*DesA showed a moderate substrate preference for lysine (K_m = 0.17 mM, k_{cat} = 0.26 s^{-1}) compared to ornithine (K_m = 0.13 mM, k_{cat} = 0.14 s^{-1}), while *Gr*DesA exhibited specificity for lysine (K_m = 0.13 mM, k_{cat} = 1.2 s^{-1}) compared to ornithine (K_m = 2.9 mM, k_{cat} = 0.18 s^{-1}). The maximum decarboxylase activity of *Ps*DesA was achieved at pH 7.5 at 35 °C, although *Ps*DesA was stable up to 40°, its relative activity decreased significantly at 50 °C. The temperature optimum (40 °C) and thermostability of *Gr*DesA were likewise, but it exhibited maximum activity at pH range 8.0–8.5, and sharply decreased outside of this range. The expression and characterization of these two decarboxylases provides insight into the biosynthetic pathway of desferrioxamines from *G. rubripertincta* and *P. simplex* and supports the functional annotation of related pathways.

1. Introduction

The poor solubility of iron in aqueous solution under physiological pH and aerobic conditions limits its bioavailability, nonetheless, bacteria have evolved a variety of strategies to overcome iron limitation. One of the most successful strategies is the production and secretion of low-molecular-weight metal chelating compounds termed siderophores [1]. Upon iron binding, the siderophore-iron complex is transported into the cell by an APT-binding cassette (ABC) transport system [2]. Iron is then removed from the siderophore-complex by either reductive or hydrolytic mechanisms [3,4]. Initially, two biosynthetic pathways were known for these compounds: one dependent on non-ribosomal peptide synthetases (NRPS), the other on polyketide synthetases [5]. A decade ago, another siderophore assembly mechanism has been recognized based on NRPS independent enzymes (NIS) [6,7]. Instead of peptide bonds, amide bonds link the altering diamine and dicarboxylic acid building blocks. The first siderophore discovered to be assembled by this NIS pathway was aerobactin from *Escherichia coli* K-30, which was found to be dependent on the two siderophore synthase superfamily enzymes *iucA* and *iucC* [8,9].

Studies of other NIS pathway gene clusters indicated that the biosynthesis of siderophores like alcaligin [10], rhizobactin 1021 [11], achromobactin [12], bisucaberin [13], vibrioferrin [14] and desferrioxamines (DFO) [15] involves at least one siderophore synthetase with a high similarity to IucA/IucC [6]. In some of these NIS pathways, decarboxylases play an important role, often catalyzing the initial step of the siderophore biosynthesis (Fig. 1).

The first step in the biosynthesis of alcaligin in *Bordetella pertussis* and putrebactin in *Shewanella putrefaciens* is the decarboxylation of ornithine to yield putrescine (1,4-diaminobutane) mediated by an

* Corresponding author.
** Corresponding author. Environmental Microbiology, Institute of Biosciences, TU Bergakademie Freiberg, Leipziger Str. 29, 09599, Freiberg, Germany.
E-mail addresses: marika.hofmann90@gmail.com (M. Hofmann), dirk.tischler@rub.de (D. Tischler).

https://doi.org/10.1016/j.abb.2020.108429
Received 23 April 2020; Received in revised form 19 May 2020; Accepted 20 May 2020
Available online 30 May 2020
0003-9861/ © 2020 Elsevier Inc. All rights reserved.

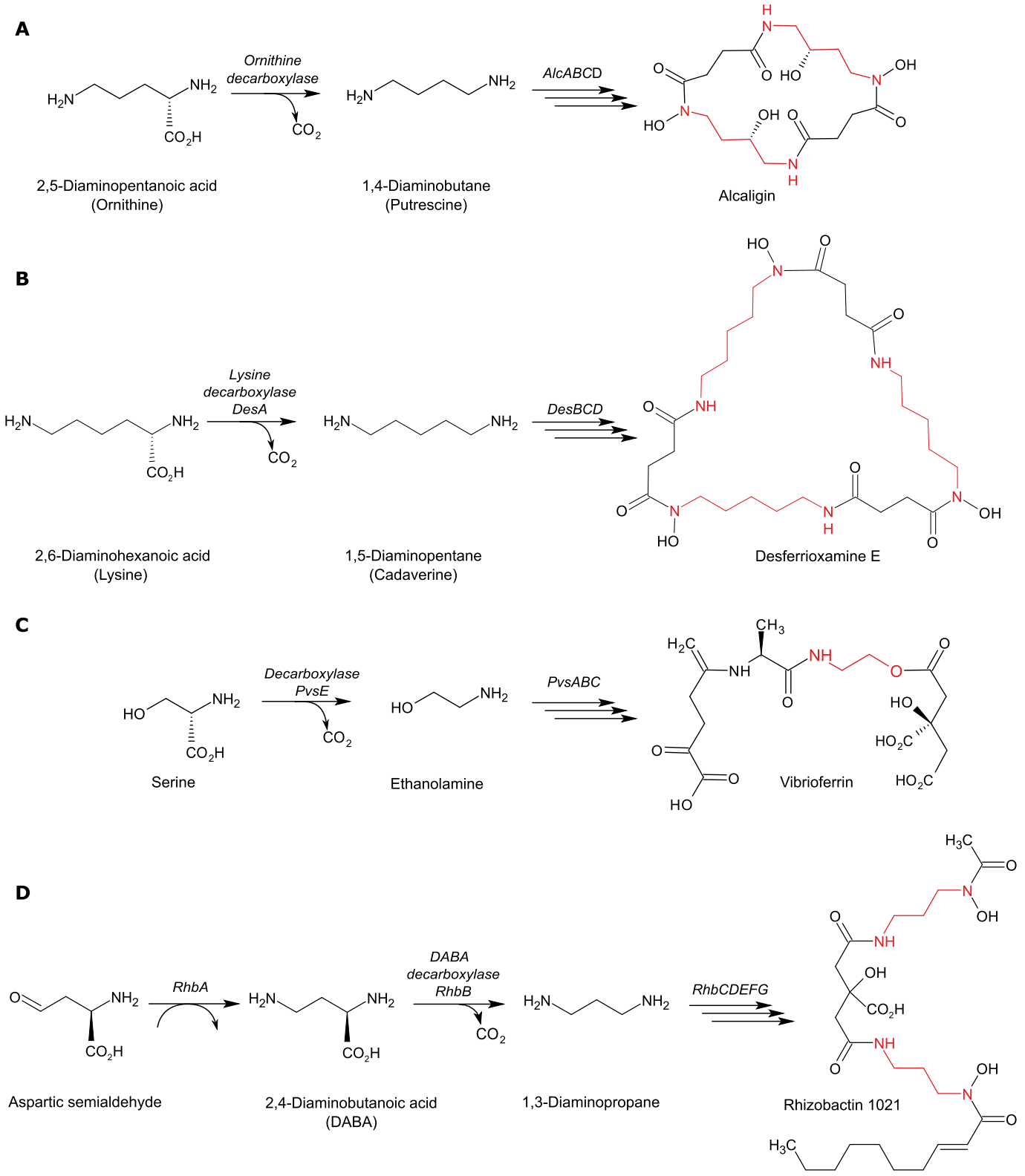

Fig. 1. Decarboxylation steps of the proposed NIS biosynthetic pathways for different siderophores biosynthesis. (**A**) Alcaligin is produced by *Bordetella pertussis* [6,10], (**B**) desferrioxamine E by *Streptomyces coelicolor* A3(2) [15], (**C**) vibrioferrin by *Vibrio parahaemolytics* [6,14]and (**D**) rhizobactin 1021 by *Sinorhizobium meliloti* 1021 [6,11].

ornithine decarboxylase (ODC) [10,16]. The inhibition of the decarboxylase in *S. putrefaciens* lead to the production of unnatural siderophores [16]. The ODC of *B. pertussis* is not part of the alcaligin gene cluster *alcABCD* [10] and shows parallels to the histidine decarboxylase from *Vibrio anguillarum*, which is involved in the biosynthesis of anguibactin, but only a partial protein sequence of this ODC is available [17–19]. Another decarboxylase gene (*pvsE)* was found to be involved in the biosynthesis of vibrioferrin in *Vibrio parahaemolytics*. *PvsE* encodes a PLP-dependent decarboxylase which catalyzes the decarboxylation of serine [14]. Although several genes encoding for

decarboxylase homologues have been identified within the siderophore biosynthesis gene clusters [20,21], only a couple of decarboxylase activities have been demonstrated. In *Streptomyces pilosus,* a lysine decarboxylase was identified to direct the desferrioxamine biosynthesis and some biochemical and kinetic properties were reported [22]. Subsequently, the respective lysine decarboxylase gene, was cloned and overexpressed, although the sequence of this gene was apparently not reported or deposited in the database [23]. It has also been reported a L-2,4-diaminobutanoic acid (DABA) decarboxylase (DC), linked to a DABA acetyltransferase (AT) from the cyanobacterium *Anabaena variabilis*, to preferentially catalyze the decarboxylation of DABA but also accepting L-ornithine and L-lysine as substrates [20]. *A. variabilis* is known to synthesize the siderophore schizokinen, which is based on 1,3-diaminopropane [24]. Additionally, Burell and coworkers investigated the enzyme DesA from *Strepomyces coelicolor*. DesA catalyzes the decarboxylation of L-lysine to cadaverine (1,5-diaminopentane), the first step of the biosynthesis of the siderophores DFOB, $DFOG_1$ and DFOE. DesA did not exhibit any sequence homology to known lysine decarboxylases [20]. Instead, it showed high similarity to DABA DCs, which are usually involved in the 3-diaminopropane biosynthesis together with DABA ATs. Characterized DABA DCs absent in the NIS biosynthetic gene cluster are reported from organisms like *A. baumannii* [25], *H. influenza* [26], *Klebsiella aerogenes* and *Serriatia marcescens* [27]. Therefore DesA was described as a new type of lysine decarboxylases (LDC) and it was hypothesized, that DABA DC homologues present in the siderophore biosynthetic gene cluster in the absence of DABA AT ORFs would be LDC [20].

Recently, the siderophore producing gene clusters were identified in the soil organisms *Gordonia rubripertincta* CWB2 and *Pimelobacter simplex* VkMAC-2033D [28]. Both organisms are known to produce desferrioxamine siderophores. Siderophores DFOB, desferrioxamine E, desferrioxamine G_1, biscucaberin and bisucaberin B have been found in the supernatants of *G. rubripertincta* cultures [29]. The siderophores of *Pimelobacter* strain VkMAC-2033D have not been described, but the close relative *Pimelobacter simplex* 3E is known to produce the siderophore desferrioxamine D [30]. As shown in Fig. 2 the siderophore gene clusters of both organisms contain the typical genes *desA*, *desB*, *desC*, *desD* and *desG* directing the DFO synthesis as well as *desE* and *desF* which are involved in siderophore binding and transport [21,31,32]. However, *desF* is only present in the *des* gene cluster in *G. rubripertincta*. The DesB homologue from *G. rubripertincta* was characterized as a functional diamine monooxygenase in a previous study and named GorA [33].

The decarboxylases *Gr*DesA and *Ps*DesA are homologues of DesA from *S. coelicolor* and represent the aforementioned new type of LDC. Limited knowledge is available regarding the LDCs and questions remain to be solved with respect to its activity and substrate specificity. Giving the fact that LDCs catalyze the initial step in the siderophore biosynthesis, these enzymes are of particular importance and there is a need for increasing the available information. Furthermore, to the best of our knowledge, studies on LDCs present in the siderophore gene cluster of *Gordonia* and *Pimelobacter* species have not been reported. Herein we present a phylogenetic analysis, cloning and heterologous overexpression of the two *desA* homologues *grdesA* and *psdesA*, as well as the characterization of the enzyme activity, cofactor identity, temperature and pH stability.

2. Materials and methods

2.1. Bacterial strains, plasmids and cloning

The genes *psdesA* from *Pimelobacter simplex* VkMAC-2033D and *grdesA* from *Gordonia rubripertincta* CWB2 were optimized according to the codon usage of strain *Acinetobacter* sp. ADP1 (allowing higher gene expression levels within *E. coli*), synthetically produced (Ebersberg, Germany) and received in pET16b vector as reported earlier [34]. The decarboxylases are listed in GenBank under the protein accession numbers MN699956 (*Ps*DesA) and MN699957 (*Gr*DesA), respectively. Since the expression of *psdesA* failed in the pET vector system, the gene was transferred to another expression vector. *PsdesA* was amplified by PCR using primers *psdesA_SgfI_fw* and *psdesA_PmeI_rev* and the plasmid was transformed into *E. coli* BL21 (DE3). All plasmids used in this study are listed in Table 1. The resulting PCR product was running on a 0.8% agarose gel, the DNA band was excised and purified using a Qiagen PCR clean-it kit. The purified DNA was digested with the restriction enzymes SgfI and PmeI and ligated into the expression vector pVP56K [35], which was previously treated with SgfI and PmeI to provide a linearized vector backbone. The ligation product was transferred into *E. coli* DH5α for plasmid propagation. Plasmids pET16b_*grdesA* and pVP56K_*psdesA* were transformed into *E. coli* BL21 (DE3) competent cells.

2.2. Heterologous expression and protein purification

Genes were expressed using autoinduction medium (100 μg/mL ampicillin) in Fernbach flasks as described elsewhere [36]. *PsdesA* was expressed as fusion-protein via *N*-terminal fusion with a 6xHis-tagged maltose binding protein (MBP). Cultures of *E. coli* BL21_pET16b_*grdesA* and *E. coli* BL21_pVP56k_*psdesA* were incubated in autoinduction medium at 37 °C until the OD_{600} reached a value of about 4 followed by an 18 h expression at 18 °C while constantly shaking at 250 rpm [37]. Cells were harvested by centrifugation (5000 × *g*; 30 min) and the resulting cell pellet was stored at −80 °C. For purification, cells were resuspended in buffer A1 (25 mM HEPES, 300 mM NaCl, 5 mM imidazole, pH 7.5) containing 40 μg/mL of lysozyme and 20 μg/mL each of DNAse and RNAse. The resuspended cells were disrupted by 15 min sonification (pulse on 5 s, pulse on 10 s, amplitude 70%) and cell debris were removed afterwards by centrifugation at 17,000 × *g* for 1 h at 4 °C. The protein purification was performed with two in tandem 5 mL His Trap FF (GE Healthcare) in one step for *Gr*DesA or two steps for *Ps*DesA. The supernatant containing *Gr*DesA was loaded into the column previously equilibrated with buffer A1. Nonspecific proteins were removed by washing the columns with 10% buffer B (25 mM HEPES, 300 mM NaCl, 300 mM imidazole, pH 7.5). *Gr*DesA was eluted with 100% buffer B. Supernatant containing MBP-*Ps*DesA fusion-protein was loaded into the column previously equilibrated with buffer A2 (25 mM HEPES, 300 mM NaCl, 5 mM imidazole, pH 7.5). MBP-*Ps*DesA was purified as described for *Gr*DesA. To remove the MBP from the target protein *Ps*DesA, the fusion-protein was cleaved with tobacco etch virus (TEV) protease (0.5 mg/mL) and the sample was dialyzed overnight against 20-fold volume of buffer C (25 mM HEPES, 300 mM NaCl, pH 7.5) to remove remaining imidazole. Cleaved protein was separated by IMAC, using buffer C as binding buffer. The target protein *Ps*DesA eluted with the flow-through. Collected samples of *Ps*DesA and *Gr*DesA were transferred into storage buffer (100 mM phosphate buffer, 50 mM NaCl, pH 7.5), and concentrated using ultrafiltration device with MWCO of 30 kDa (Millipore). Purified, concentrated protein was frozen as beads in liquid nitrogen and stored at −80 °C.

2.3. Protein determination

Purity and subunit molecular mass were estimated by sodium dodecyl sulfate polyacrylamide gel electrophoresis (SDS-PAGE). Protein concentration was determined using Bradford reagent and pre-diluted protein assay standards BSA Set (Thermo Scientific).

The hydrodynamic properties of the enzymes were analyzed at room temperature by using a Superdex 200 HR10/300 GL column attached to an Äkta Prime Plus FPLC system (GEHealthcare). 50 mM phosphate buffer (pH 7.0) containing 150 mM NaCl was used as mobile phase at a flow rate of 0.5 mL/min 100 μL and 200 μL protein was injected in each run, respectively. For calibration, the following proteins were used: Ovalbumin (43 kDa), Conalbumin (75 kDa), Aldolase (158 kDa), and Ferritin (440 kDa). Blue Dextran (2000 kDa) was used to

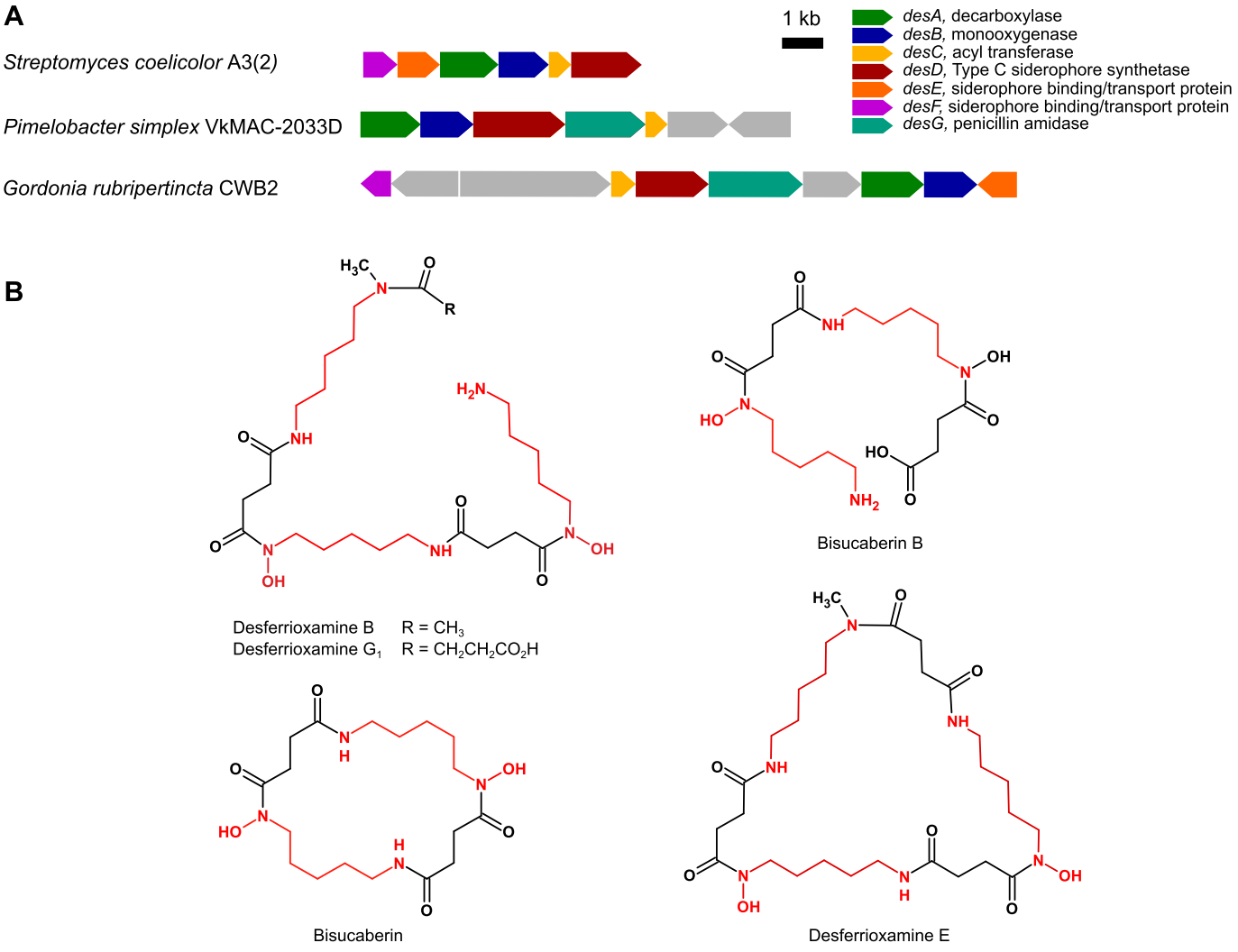

Fig. 2. (**A**) Organization of the desferrioxamine biosynthetic gene clusters of *Streptomyces coelicolor* A3(2), *Pimelobacter simplex* VkMAC-2033D and *Gordonia rubripertincta* CWB2. The prototypic genes *desABCD* (first identified in *S. coelicolor*), encode the PLP dependent decarboxylase (DesA), a lysine monooxygenase (DesB), an enzyme similar to a CoA-dependent acyl transferase, which is assumed to catalyze the acylation of *N*-hydroxycadaverine and a Typ C siderophore synthetase homologue (DesD). DesG was noticed recently to be present in some Actinobacteria and encodes an enzyme similar to a penicillin amidase [21], which is proposed to be responsible for the synthesis of aryl-substituted hydroxamic acids via acylation of *N*-hydroxycadaverine. (**B**) Structure of the produced siderophores of all three bacteria. Lysine backbones are indicated in red. For interpretation of the references to color in this figure legend, the reader is referred to the Web version of this article.

Table 1
Plasmids used in this study.

Sample	Relevant characteristic(s)	Source or reference
Strains		
E. coli DH5α	*fhuA2 Δ(argF-lacZ) U169 phoA glnV44 Φ80 Δ(lacZ)M15 gyrA96 recA1 relA1 endA1 thi-1 hsdR17*	NEB
E. coli TurboCell BL21(DE3)pLysS	F- *ompT hsdS*$_B$ (r_B- m_B-) *gal dcm* (DE3) pLysS (Cm^r)	Genlantis
Plasmids		
pVP56k	7253 bp, adds N-terminal 8xHis, MBP, Kan^r	[35]
pET16b_*psdesA*	pET 16b (5711 bp) and *psdesA* (1479 bp) from *Pimeobacter simplex* VkMAC-2033D as insert	MWG Eurofins
pET16b_*grdesA*	pET 16b (5711 bp) and *grdesA* (1547 bp) from *Gordonia rubripertincta* CWB as insert	MWG Eurofins
pVP56k_*psdesA*	*psdesA* (1497 bp SgfI/PmeI fragment) cloned into pVP56k	This study
Primers		
psdesA_SgfI_fw	5′-AGGAGCGATCGCCATGCCGCAATTGCCGTTGC ATCAC-3′[a]	This study
psdesB_PmeI_rev	5′- GGTTGTTTAAACGCGACCACCTCCAGCGCTG-3′[a]	This study

[a] SgfI or PmeI restriction site underlined.

determine the void volume. Apparent M_r values of *Ps*DesA was obtained from a graph where the partition coefficient (K_{av}) of the standard proteins was plotted against log M_r.

2.4. Cofactor analysis

Absorbance data were recorded using an Agilent 8453 UV visible spectrometer. The identity of pyridoxal phosphate in the protein sample was verified using a multiple reaction monitoring (MRM) method generated with an AB Sciex 3200 Q Trap mass spectrometer. Commercial PLP was used as standard. HPLC separation utilized a Kinetex 2.6 μm, 100 Å, 100 × 2.1 mm HILIC column from Phenomenex. Solvents A and B were mixtures of acetonitrile:50 mM ammonium formate in water (pH 3.2) (ratio 9:1) and acetonitrile:50 mM ammonium formate in water (pH 3.2) (ratio 5:4:1). The HPLC gradient was generated and flow rate maintained at 200 μL/min utilizing an Agilent 1100 series HPLC. Following an equilibration for 13 min at 90% A, sample was injected using an Agilent 1100 series autosampler. After injection of sample, 2 min at 90% A was followed by a 9-min gradient to 100% B, then a 10-min hold at 100% B at which time the gradient was returned to 90% A for subsequent equilibration of the HILIC column. Analysis were carried out using mass spectroscopy with a 5500 V ionization source at 120 °C source temperature. CAD gas was set to medium and curtain, gas 1 and gas 2 were 10, 15 and 10, respectively. The declustering potential was 51 V, entrance potential was 5 V, collision cell entrance potential was 16 V and collision cell exit potential was 4 V. Both quadrupoles were operated at unit resolution. The three fragments of the protonated PLP ion (m/z = 248.05) monitored were 150.3 (collision energy 21 V), 122.1 (collision energy 31 V) and 106.1 (collision energy 31 V), each for 150 ms dwell time.

2.5. Enzyme activity assay

Decarboxylase activity of *Gr*DesA and *Ps*DesA was determined colorimetrical using 2,4,6-trinitrobenzenesulfonic acid (TBNS) to give colored trinitrophenyl-putrescine (TNP-PUT) [38,39]. A standard assay contained 3 mM ornithine and 150 mM phosphate buffer (pH 7.1) in a total volume of 30 μL. The assay was started by the addition of enzyme to a final concentration of 6.5 μM (*Ps*DesA) and 22 μM (*Gr*DesA), respectively. 75 nM PLP were added to *Gr*DesA containing samples. After 20 min at 30 °C the reaction was quenched by adding 20 μL 10% perchloric acid. The reaction mixture was assayed for its content of putrescine using the spectrophotometric assay similar to the modified spectrometric ODC assay described by M.E.-Legaz [39], but in a scale 1:10. The downscaling makes it applicable for the measurement in microtiter plates. Putrescine concentration was calculated using the calibration curve shown in Fig. S1 (Supporting Information).

The optimum temperature of enzyme activity was determined by performing the standard assay at temperatures between 10 and 70 °C (after pre-incubation of the reaction mixture). The optimum pH-value for ornithine conversion was determined by using phosphate buffer varying between pH 5.7 and 9.0 and Britton-Robinson buffer varying between pH 7.5 and 9.5 in the assay standard. Thermal stability was measured by incubating the enzymes at temperatures between 20 and 60 °C. Samples were taken periodically and assayed for residual activity using the standard assay.

2.6. Product determination using UPLC

Product formation, kinetic parameters, buffer preference and substrate specificity were determined *via* UPLC analysis. A standard assay for the determination of kinetic parameters contained 50 mM HEPES buffer (pH 8.0), varying substrate concentrations and 2 μM (*Ps*DesA) and 1 to 6,7 μM (*Gr*DesA) enzyme, respectively. The reaction was stopped after 5 min incubation at 30 °C by heating the sample at 95 °C for 10 min. To determine the optimal buffer, the assay was carried out with Tris buffer, phosphate buffer and HEPES buffer, each with a concentration of 50 mM and a pH of 8.0. After centrifugation (5 min, 13,000 × *g*) 65 μL of the supernatant was mixed with 12.5 μL 200 mM borate (pH 8.0). For derivatization, 1.6 μl of 150 mM 9-fluorenylmethyl chloroformate (Fmoc-Cl) was added and the reaction was allowed to proceed 5 min at room temperature shaking at 600 rpm. To remove remaining derivatizing reagent, 79 μL of 53 mM 1-aminoadamantane (ADAM) was added. After an additional chilling at room temperature for 15 min, the reverse phase UPLC analysis was carried out on an AccQ-Tag Ultra RP Column (130 Å 1.7 μm, 2.1 × 100 mm, 43 °C) running a gradient from 30 to 100% over 10 min (solvent: A 0.1% TFA/H_2O; solvent B: 0.1% TFA/MeCN). Product identity was confirmed by coelution with a similar Fmoc-derivatized putrescine or cadaverine standard. Kinetic data are listed in the STRENDA data base under the Strenda ID NXSUD (GrDesA) and TFZ7HT (PsDesA), respectively.

Next to L-lysine and L-ornithine the substrates D-lysine, D-ornithine, 2,4-diaminobutanoic aid (DABA), arginine and histidine were tested with *Gr*DesA and *Ps*DesA for decarboxylase activity. Analytics were done using ortho-phtalaldehyde (OPA) derivatization. Therefore 70 μL sample were mixed with 35 μL derivatization solution (10 mg/mL OPA, 100 mM borate buffer pH 9.2, 10 μL/mL mercaptoethanol in methanol). After 1 min incubation, 900 μL of neutralization solution (20 mM sodium acetate pH 6.1 with 20% v/v acetonitrile were added. The HPLC analysis were carried out using a Eurosphere C_{18} (4 × 125 mm) column in Ultimate 3000 HPLC system. The method consisted on an isocratic elution with 30% acetonitrile in water during 10 min.

3. Results

3.1. Phylogenetic analysis

The desferrioxamines siderophore biosynthetic gene clusters of the Actinobacteria *P. simplex* VkMAC-2033D and *G. rubripertincta* CWB contain each a decarboxylase, hypothesized to be responsible for the decarboxylation of lysine to cadaverine in the DFO biosynthesis. antiSMASH annotation predicted both genes to be DABA DCs not adjacent to DABA ATs and confirmed the predicted function as lysine decarboxylases as described by Burrell [20]. Pairwise alignments of amino acid sequences of *Ps*DesA and *Gr*DesA with related decarboxylases from *S. coelicolor*, *A. variabilis* and *A. baumannii*, which has been

Table 2
Results from pairwise alignments of the decarboxylases involved in siderophore synthesis from *P. simplex*, *G. rubripertincta* with related enzymes.

Enzyme	*Ps*DesA		*Gr*DesA	
	Identity (%)	Similarity (%)	Identity (%)	Similarity (%)
LDC DesA (*S. coelicolor* A3(2)	56	67	38	54
DABA DC (*A. variabilis*)	41	59	39	56
DABA DC (*S. meliloti*)	42	58	39	54
DABA DC (*A. baumannii*)	41	61	33	51
LDC (*Plesiocystis pacifica* SIR)	39	51	52	66
DABA DC (*Frankia alni* ACN)	39	51	42	54

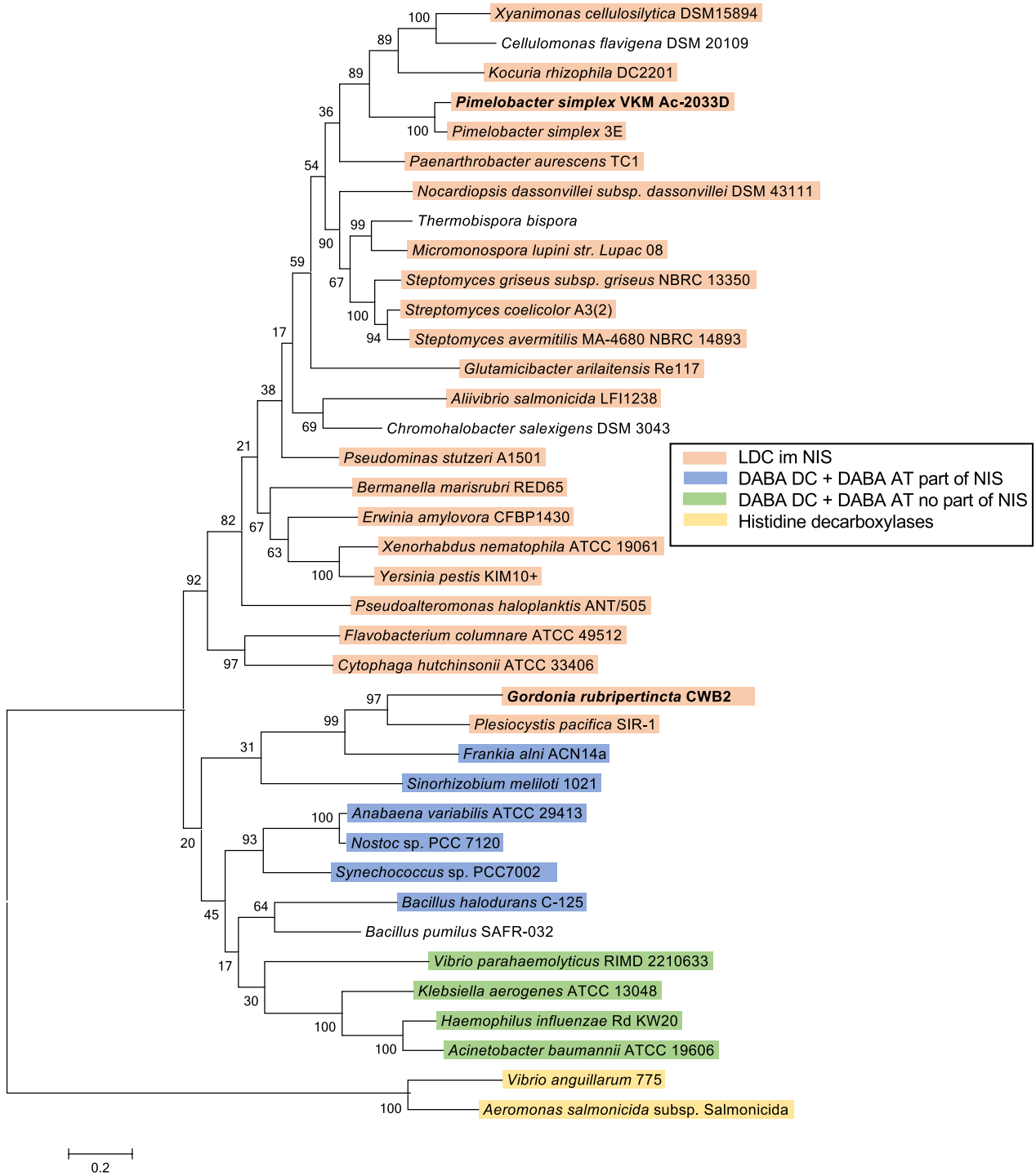

Fig. 3. Phylogenetic (Neighbor Joining) tree of *Ps*DesA from *P. simplex* VKM AC-2033 D, *Gr*DesA from *G. rubripertincta* and related LDC and DABA DC homologues mostly present in the NIS gene cluster. The Neighbor-Joining distance tree was solved by using Mega 6.06 with ClustalW alignment method. The different colors indicate their (potential) function as LDC in NIS (orange), DABA DC linked to a DABA AT as part of the NIS (blue), DABA DC linked to a DABA AT, but not part of the NIS (green) and histidine decarboxylase (yellow). For interpretation of the references to color in this figure legend, the reader is referred to the Web version of this article.

described to be active, revealed significant similarities (listed in Table 2). However, *Gr*DesA was found to be closer related to uncharacterized decarboxylases like the DC *of Plesiocystis pacifica* SIR-1 and the DABA DC from *Frankia alni* ACN 14a.

An alignment of active related decarboxylases as well as uncharacterized homologues (present in a functional siderophore cluster) were used to construct a phylogenetic tree and their relationship to *Ps*DesA und *Gr*DesA (Fig. 3). As described in a previous study [20], the homologues separate into two clades: one including the functional LDC type homologues (DABA DC without DABA AT in NIS), whereas the other clade contains mostly DABA DC homologues adjacent to DABA ATs, some of them in NIS cluster, the others not. *Ps*DesA clusters within the first clade, whereas *Gr*DesA on the other hand is localized away from the functional LDCs within the second clade.

3.2. Gene expression and purification

The two decarboxylase genes *psdesA* and *grdesA* were codon optimized for expression in *E. coli* [34] and obtained by gene synthesis. The synthetic genes had been successfully used to create the respective expression constructs pET16bp_*grdesA* and pVP56K_*psdesA*. Proteins were heterologously expressed in *E. coli* BL21 (DE3) pLysS either, as *N*-terminal His_{10}-tagged protein (*Gr*DesA) or in case of *Ps*DesA as *N*-terminal His_8-tagged fusion protein with maltose binding protein (MBP). Around 18 g of *grdesA*-containing cells and 8 g of *psdesA*-containing cells were obtained per liter of culture medium. Purified proteins were found to be stable in 100 mM phosphate buffer with 50 mM NaCl (pH 7.5) and were stored in this buffer at −80 °C.

3.3. Purification and enzyme stability

*Gr*DesA purification was achieved by immobilized nickel ion affinity chromatography (IMAC) resulting in highly purified protein that was used for further studies. The molecular masses of *Gr*DesA was estimated to be 57 kDa by SDS-PAGE (Supporting Information, Fig. S2), as expected from the deduced amino acid sequence (535 acid residues, with a theoretical mass of 54.459 kDa plus 1.389 kDa His_{10}-tag). Purification yielded 0.8 mg protein per gram of cells. In order to determine suitable conditions for enzyme assays, various conditions were tested. For those tests, the enzyme activity was determined using the colorimetric TBNS assay as described in materials and methods.

The addition of pyridoxal-5-phosphate (PLP) was found to be necessary for enzyme activity. Without PLP addition, no enzyme activity was observed. *Gr*DesA showed high activity (> 70%) between 30 and 45 °C with an optimum at 40 °C (Fig. 4). Temperature stability was examined by incubating the enzyme at different temperatures for 30 min and thereafter the residual activity was determined at standard assay conditions. Enzyme activity kept increasing at temperatures up to 40 °C. However, enzyme activity decreased rapidly at higher temperatures. The enzyme showed maximum activity at pH 8.5 and a low activity (< 25%) at pH values lower than 7.0 and higher than 9.5.

*Ps*DesA was purified using a two-step IMAC purification process. First, the polyhis-tagged MBP-fusion protein was isolated from the crude extract. After cleavage of the fusion protein, *Ps*DesA was separated from polyhis-tagged MBP in the second purification step. High purity, successful cleavage and expected molecular weight (493 amino acid residues, with a theoretical mass of 53.086 kDa) was confirmed by SDS-PAGE (Fig. 5A).

Purification yielded 1.4 mg protein per gram of cells. Purified *Ps*DesA showed a yellow color, indicating a tightly bound cofactor. The UV–Visible spectrum of the purified enzyme solution of *Ps*DesA showed highest absorption at 421 nm. This bound is characteristic of PLP bound as an aldimine [40]. After denaturation, the peak blue shifted and showed a maximum at 390 nm similar to free PLP (Fig. 5B). Multiple reaction monitoring (MRM) analysis of the enzyme identified the yellow cofactor unambiguously as PLP (Supporting information, Fig. S3).

Activity tests with different buffers at pH 8.0 revealed that the decarboxylase is most active in HEPES and phosphate buffer to a similar extent. In Tris buffer the enzyme was around 75% active. The optimal pH for *Ps*DesA activity was observed at pH 7.5. *Ps*DesA exhibited a high tolerance towards pH variation and retained residual activities > 35% in a range of pH 5.5 to 9.0 (Fig. 6). High enzyme activities (> 70%) was observed between 30 and 45 °C with an optimum at 35 °C. *Ps*DesA showed a high stability without activity loss at temperatures up to 40 °C. Higher temperatures led to a rapid activity decrease (see Fig. 7).

3.4. Gel filtration and substrate specificity

To validate the oligomeric state of the enzyme, a size exclusion chromatography under non-denaturizing conditions was performed in duplicate. The results show that *Gr*DesA is mostly present in a dimeric form (141 kDa calculated from elution volume, 57 kDa subunit size) and *Ps*DesA in a tetrameric form (235 kDa calculated from elution volume, 53 kDa subunit size). However, the elution peak of *Ps*DesA showed a shoulder indicating, that the enzyme might occur in a second hydrodynamic state as well.

To examine the activity of both enzymes, steady state kinetics with L-lysine were analyzed and kinetic parameters determined. In addition to L-lysine, the decarboxylase activity with L-ornithine was of special interest, since the previous characterized diamine monooxygenase GorA of the NIS siderophore gene cluster of *G. rubripertincta* CWB2 showed very high activity towards the corresponding substrate putrescine, which was even higher than the activity towards cadaverine [33]. DesB is suggested to catalyze the second step in the siderophore

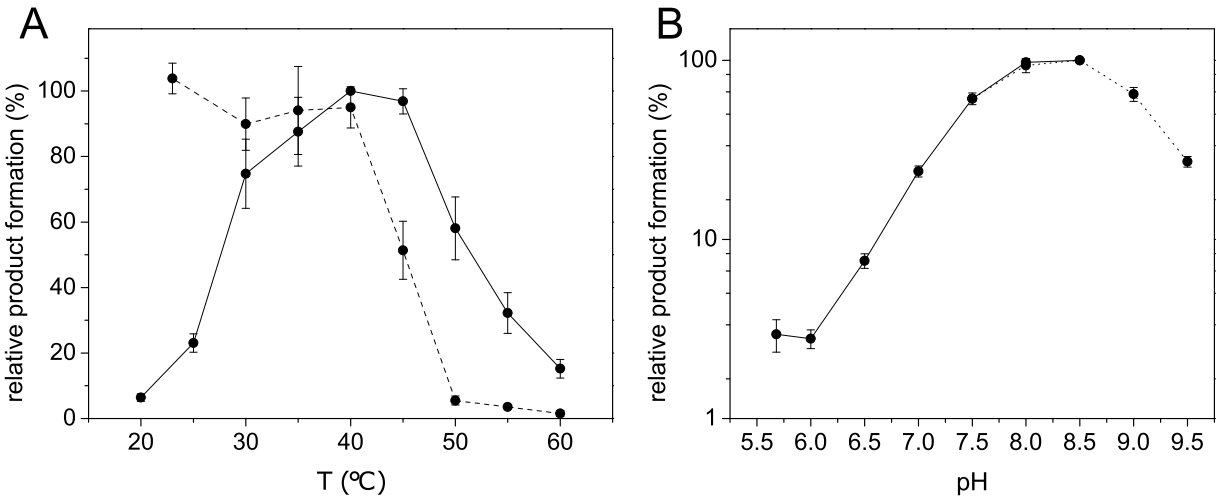

Fig. 4. Effect of pH and temperature on product of *Gr*DesA. **(A)** Temperature optimum (solid line) and stability (dashed line) of *Gr*DesA were measured using standard TBNS-assay conditions with 150 mM phosphate buffer after 20 min at various temperatures (20–60 °C). Samples for temperature stability determination were pre-incubated for 20 min at temperatures ranging from 20 °C to 60 °C and afterwards analyzed at standard conditions (30 °C). The maximal product formation was observed at 40 °C with (24 μM putrescine/μM enzyme). **(B)** Normalized activity-pH plot. The enzyme activity was measured using TBNS-assay standard conditions with different pH values in phosphate buffer (pH 5.6–8.5, solid line) and Britton-Robinson buffer (7.5–9.5, dotted line). The maximal product formation was observed at pH 8.5 with (47 μM putrescine/μM enzyme). All measurements were determined in triplicates. The relative activity is expressed as a percentage of the activity observed at 40 °C or pH of 8.5, respectively.

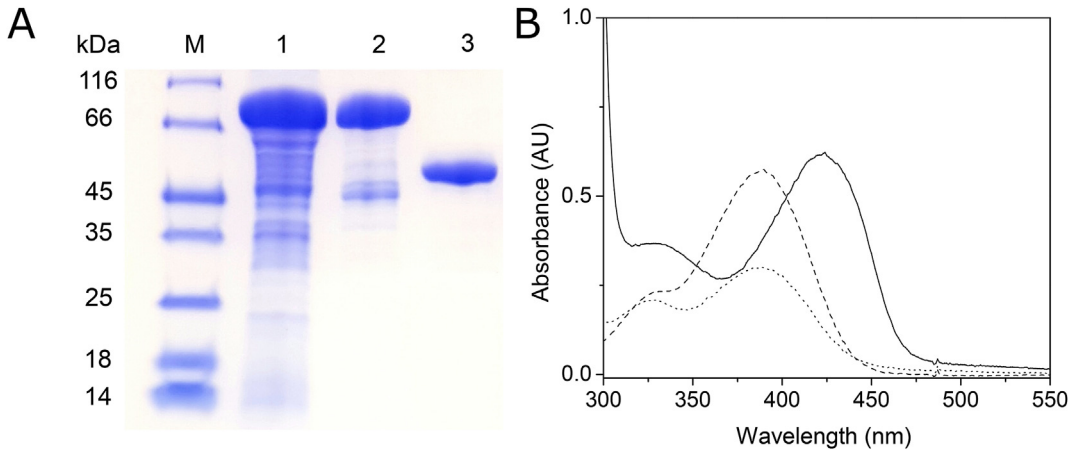

Fig. 5. (A) SDS-Page of purification process of *Ps*DesA. M: Protein marker, lane 1: crude extract, lane 2: fusion protein after IMAC 1 (fusion protein ca. 100 kDa), lane 3: purified *Ps*DesA (theoretical mass 53.086 kDa) after IMAC 2. **(B)** Absorbance spectra of purified native *Ps*DesA (solid line), supernatant of denatured *Ps*DesA (dotted) and PLP standard (94 nM, dashed line).

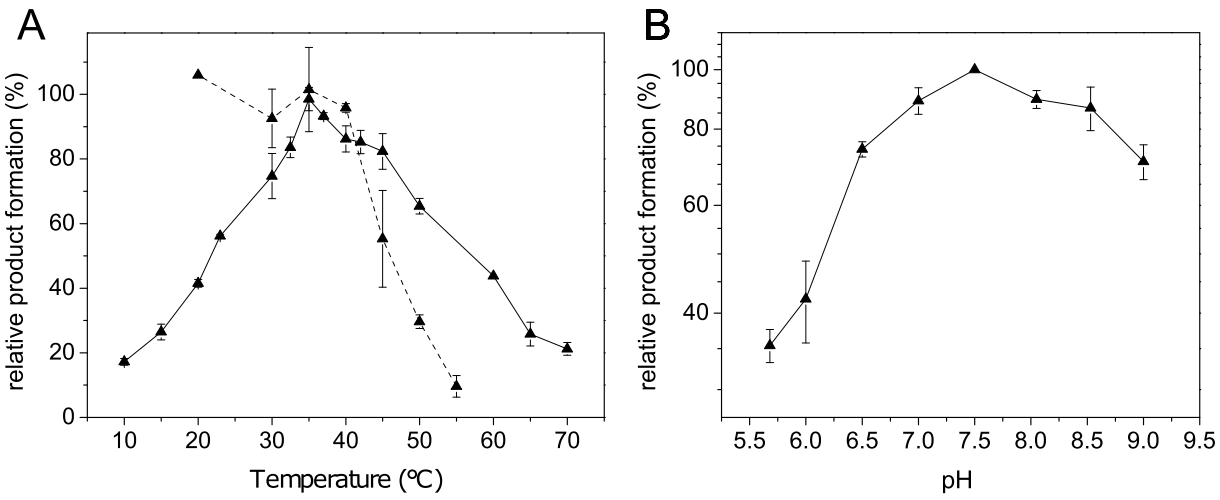

Fig. 6. Effect of pH and temperature on the relative product formation of *Ps*DesA. **(A)** Temperature optimum (solid line) and stability (dashed line) were measured using standard TBNS-assay conditions with 150 mM phosphate buffer after 20 min at various temperatures. Temperature stability samples were pre-incubated 30 min at temperatures ranging from 20 °C to 55 °C and afterwards analyzed at standard conditions (30 °C). The maximal product formation was observed at 35 °C with (77 μM putrescine/μM enzyme). **(B)** Normalized activity-pH plot. The enzyme activity was determined using TBNS-assay standard conditions with different pH values in phosphate buffer. The maximal product formation was observed at pH 7.5 with (91 μM putrescine/μM enzyme). All measurements were done in triplicates. The relative activity is expressed as a percentage of the activity observed at 35 °C or pH of 7.5, respectively.

biosynthesis of *G. rubripertincta* after the decarboxylation. *Gr*DesA showed activity towards the substrates L-lysine and L-ornithine (Fig. 8), exhibiting an indisputable preference for L-lysine. The decarboxylase from *G. rubripertincta* was determined to have a K_m values of 0.13 ± 0.03 and a k_{cat} value of 1.2 ± 0.1 s^{-1} for L-lysine and a K_m of 2.9 ± 0.24 mM (k_{cat} = 0.18 ± 0.01 s^{-1}) for L-ornithine. *Ps*DesA on the other hand showed activity with both, L-lysine and L-ornithine in an almost similar extent. Here k_{cat} was determined to be 0.26 ± 0.01 s^{-1} (K_m = 0.17 ± 0.02 mM) with L-lysine, with L-ornithine the enzyme showed a k_{cat} value of 0.16 ± 0.01 s^{-1} and a K_m of 0.13 ± 0.02 mM (Table 3). Furthermore, the acceptance of D-lysine, D-ornithine, DABA, arginine and histidine as substrates by both enzymes was investigated following the product formation by HPLC. Both enzymes were able to catalyze the reaction of DABA to 1,3-diaminopropane, although the decarboxylation seemed to be less effective compared to L-lysine (specific enzyme activity not determined) and to a very low extend the conversion of the D-lysine and D-ornithine (< 10%). This is in accordance to the results of the decarboxylase from *S. pilosus*, which did not accept D-Lysine as a substrate [22]. No product formation was observed with arginine and histidine as substrates for *Gr*DesA and *Ps*DesA.

4. Discussion

Lysine decarboxylases are important enzymes in the biosynthesis of microbial siderophores often catalyzing the first step in the pathways. Since siderophore production in response to iron limitation is essential for pathogenesis [41–43], characterization of the siderophore gene clusters and studying their genes and proteins could be of great importance for drug discovery. However, only little is known about the siderophore biosynthetic decarboxylases and their biochemical properties. To extend the knowledge about these enzymes, the two DesA homologues *Gr*DesA and *Pr*DesA of the two desferrioxamines producing Actinobacteria *P. simplex* VKM Ac-2033D and *G. rubriperincta* CWB2 were investigated.

The new LDC type present in the siderophore NIS gene cluster described in 2012 [20] appears as DABA DCs without an adjacent DABA AT. DABA ATs are found in many bacterial pathways, either independently from DABA DCs, like in the NIS pathway for the hydroxycarboxylate achromobactin, or as a DABA DC/DABA AT pair, where

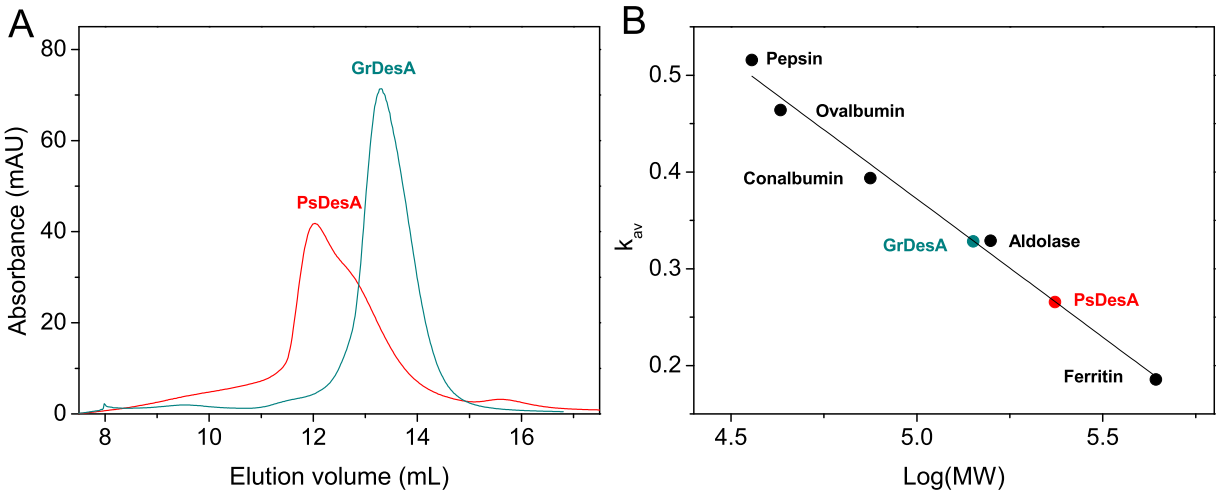

Fig. 7. Size exclusion chromatogram of *Ps*DesA (cyan) and *Gr*DesA (red) (**A**) and calibration plot including the measured target enzymes (**B**). The calibration curve prepared by plotting partition coefficient of protein standards: Pepsin (36 kDa), Ovalbumin (43 kDa), Conalbumin (75 kDa), Aldolase (158 kDa), Ferritin (440 kDa). The K_{av} value for *Ps*DesA is shown in red and for *Gr*DesA in green. The size exclusion chromatography was performed in 50 mM phosphate buffer pH 7.0 containing 150 mM NaCl. For interpretation of the references to color in this figure legend, the reader is referred to the Web version of this article.

DABA AT catalyzes the formation of DABA, the substrate for the DABA DC [44,45]. The latter are found, for example, in the NIS biosynthetic gene clusters for the biosynthesis of rhizobactin 1021 in *S. meliloti* [11] and the NRPS gene cluster for vibriobactin biosynthesis in *Vibrio cholerae* [46]. In the absence of the DABA AT the substrate DABA is not provided. Therefore it is very likely that DABA DCs lacking DABA ATs in NIS gene clusters function as the mentioned novel LDCs [20]. The two *desA* homologues *grdesA* and *psdesA* fit the criteria for that type of LDCs and the siderophores desferrioxamines and biscuberin contain lysine building blocks. This lead to the proposal that both DABA DC enzymes could be functional lysine decarboxylases. To explore this possibility, the enzymes were successfully cloned, overexpressed and purified. Activity tests of *Gr*DesA and *Ps*DesA proved their function as lysine decarboxylases and further showed activity with ornithine and DABA. Kinetic parameters of both enzymes with L-ornithine and L-lysine are listed in Table 3 along with kinetic parameters of related characterized decarboxylases.

The decarboxylation of L-lysine catalyzed by *Gr*DesA and *Ps*DesA is faster than what is reported for DesA from *S. coelicolor*, however the K_m value is lower for DesA [20]. K_m values of the lysine decarboxylase from *S. pilosus* is in a similar range than the K_m values of *Gr*DesA with L-lysine and of *Ps*DesA with both L-lysine and L-ornithine. k_{cat} values of *Gr*DesA and *Ps*DesA on the other hand were much higher with all substrates tested. However, the results might be not exactly comparable, since decarboxylase activity of the *S. pilosus* decarboxylase was measured in the cell free crude extract instead with an purified recombinant enzyme [22]. Also, the activity was assayed using ^{14}C-labelled lysine followed by trapping of the released ^{14}C-labelled CO_2 instead of measuring the product formation.

Comparing the substrate preferences between *Gr*DesA and *Ps*DesA, great differences can be noticed. While K_m values and the catalytical efficiency k_{cat}/K_m of *Ps*DesA with L-ornithine and L-lysine are similar and only a slight preference for L-lysine can be noticed, the catalytical efficiency of *Gr*DesA towards L-lysine is 158 times and the k_{cat} more than 6 times higher compared to L-ornithine. The preference for L-lysine over L-ornithine is indisputable and supports this amino acid, L-lysine, as the physiological substrate for *Gr*DesA. GorA is the DesB homologue in the siderophore NIS gene cluster of *G. rubripertincta* CWB2 and in the pathway the second functional enzyme after *Gr*DesA (33). However, GorA showed activity with a broad spectrum of diamines, but performed *N*-hydroxylation only with putrescine, cadaverine and hexamethylenediamine. Thus, it was not clear yet whether siderophore biosynthesis in strain CWB2 starts with L-lysine or L-ornithine. The highest activities of the monooxygenase GorA were detected with putrescine and the enzyme was therefore suggested to be a putrescine-monooxygenase [33]. The preference of the monooxygenase for the ornithine product putrescine stands thereby in contrast to the preference for lysine of the decarboxylase *Gr*DesA. However, the determined activities of GorA with cadaverine were still very high (90% compared to L-lysine [33]), making the *N*-hydroxylation of this substrate as subsequent step after L-lysine decarboxylation a very possible physiological function in the siderophore biosynthesis. In addition, we recently studied the substrate preference by comparing the kinetic parameters with both substrates cadaverine and putrescine. The results indicated that GorA is specific for cadaverine with a k_{cat}/K_m value of 2.6 × 10^3 s^{-1} M^{-1} compared to 6 s^{-1} M^{-1} for putrescine (unpublished). This agrees with our results, that *Gr*DesA converted DABA less effective than L-lysine and supports the suggestion, that *Gr*DesA is a functional lysine decarboxylase instead of a DABA decarboxylase.

The decarboxylation seems to be a substrate selective step in the siderophore synthesis of *G. rubripertincta*. In contrast, kinetic studies on *Ps*DesA show that this decarboxylase is not as specific. For *Ps*DesA the k_{cat}/K_m value was only 1.5-times higher for L-lysine than L-ornithine, while the values were 17-, 24- and 158-times higher for the preferred substrates of DesA from *S. coelicolor*, DABA DC from *A. variabilis* and *Gr*DesA, respectively.

The differences between *Gr*DesA and *Ps*DesA were also observed in other biochemical properties. The pH-optima showed maximal activity under neutral-alkaline conditions, which is very typical for biosynthetic decarboxylases [47] and fits to the expectations. However, while *Ps*DesA shows > 85% residual activity in the pH range of 7.0–8.5, *Gr*DesA showed only a very sharp reaction optimum between pH 8.0 and 8.5 and lost already 40% activity at pH values 0.5 higher or lower than that optimum. Another difference can be found in the binding of the PLP cofactor. *Gr*DesA was purified in the apo form, while PLP was covalently bound to *Ps*DesA. The results from size exclusion chromatography revealed, that the oligomeric state of *Gr*DesA is a dimer, while *Ps*DesA appears mostly as a tetramer. The fact that *Ps*DesA occurs also in a second hydrodynamic state might be due to buffer or salt concentration which effect the oligomerization to some extent.

The different kinetic and structural properties are also reflected in the phylogenetic analysis, which shows LDCs and DABA DCs present in the NIS gene cluster as well as some related, characterized representatives outside the NIS gene cluster (see Fig. 3, statistical analysis with 500 bootstrap replications, a consensus tree out of these 500 replications is shown). We found two main clusters, namely one

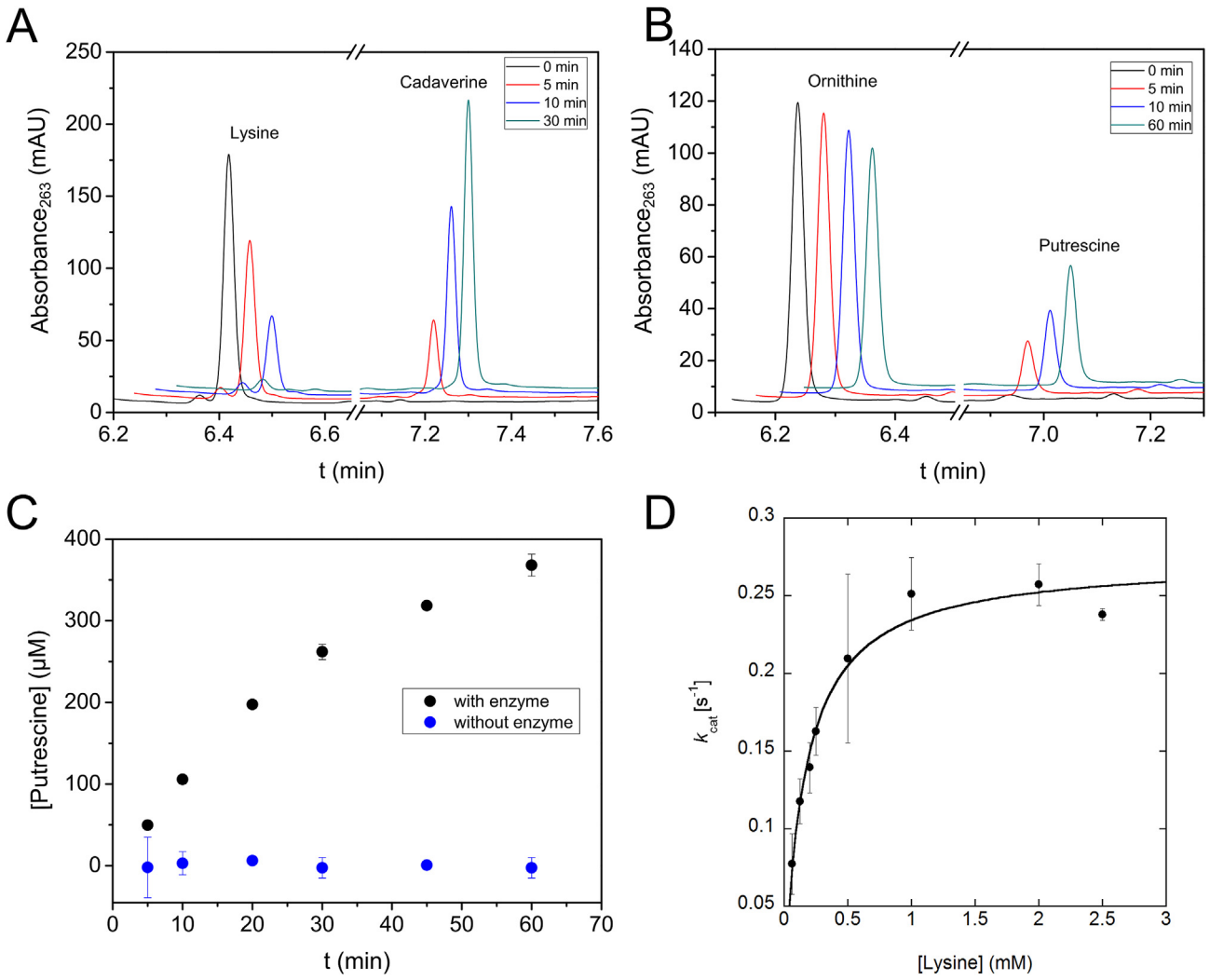

Fig. 8. Enzymatic conversion of L-lysine and L-ornithine by *Ps*DesA and *Gr*DesA. (**A**) UHPLC chromatograms of the *Gr*DesA catalyzed reaction of L-lysine (eluting after 6.42 min) to cadaverine (eluting after 7.14 min) as a function of time. The assay was carried out with 2.5 mM L -lysine in 50 mM HEPES at pH 8.0 with 75 nM PLP and 3.3 µM enzyme. (**B**) UHPLC chromatograms 0–60 min of the *Ps*DesA catalyzed reaction of L-ornithine (eluting after 6.24 min) to cadaverine (eluting after 6.94 min) after 0–60 min. The assay was carried out with 2.5 mM L-ornithine in 50 mM HEPES at pH 8.0 with 3.9 µM enzyme. (**C**) Time curve diagram of the *Ps*DesA catalyzed product formation of putrescine measured with the TBNS assay (2 mM L-ornithine). (**D**) Initial rate presented as a function of L-Lysine concentration for *Ps*DesA. The data were fitted to the Michaelis-Menten equation.

Table 3
Kinetic constants for lysine/DABA decarboxylases involved in siderophore synthesis from *P. simplex*, *G. rubripertincta* and other microorganisms.

Strain	Enzyme	Substrate	K_m (mM)	k_{cat} (s^{-1})	k_{cat}/K_m x10^3 (s^{-1} M^{-1})	Reference
Pimelobacter simplex	*Ps*DesA	L-Lysine	0.17 ± 0.02	0.26 ± 0.01	1.57 ± 0.20	This study
		L-Ornithine	0.13 ± 0.02	0.14 ± 0.01	1.06 ± 0.13	
Gordonia rubripertincta	*Gr*DesA	L-Lysine	0.13 ± 0.03	1.2 ± 0.1	9.64 ± 2.40	This study
		L-Ornithine	2.9 ± 0.2	0.18 ± 0.01	0.06 ± 0.01	
Streptomyces pilosus		L-Lysine	0.24	n.d. *	n.d.	[22]
Streptomyces coelicolor	DesA	L-Lysine	0.058 ± 0.02	0.040 ± 0.003	0.69 ± 0.20	[20]
		L-DABA	1.3 ± 0.3	0.052 ± 0.003	0.04 ± 0.01	
Anabaena variabilis	DABA DC	L-Lysine	0.30 ± 0.1	0.008 ± 0.001	0.03 ± 0.01	[20]
		L-DABA	0.54 ± 0.1	0.340 ± 0.030	0.63 ± 0.10	

n.d. = not detected, * enzyme size or decarboxylase sequence were not reported, V_{max} was determinded to be 10 nmol/mg·min.

containing LDCs and the second one containing mainly DABA DCs, which is in agreement with the phylogenetic tree published previously [20]. Although some bootstrapping values are comparably low the tree topology seems robust and thus *Ps*DesA could properly be assigned. As expected from the high similarities between *Ps*DesA and LDCs like DesA from *S. coelicolor* (56% identity), the decarboxylase from *P. simplex* clusters in the first clade along with the majority of the other LDCs. In contrast, *Gr*DesA seems to cluster in the second clade, closer to the DABA DCs, although our results led to the conclusion, that the decarboxylase of *Gr*DesA is indeed an LDC. Also, the pairwise alignments show comparably low identities and similarities with both clade representatives, LDCs from the first clade and DABA DCs in the second

clade. In general, the clustering accords with previously published phylogenetic analyses [20], but the assignment failed or seems inaccurate for a few decarboxylases like *Gr*DesA and the closely related decarboxylase from *Plesiocytis pacifica.* The results are consistent with *Gr*DesA, together with *Plesiocytis pacifica*, *Frankia alni* and *S. meliloti* form another cluster, instead of being part of the second clade. A phylogenetic analysis using a non-homologue L-lysine decarboxylase of *E. coli* K-12 as outgroup supports this suggestion (Supporting Information, Fig. S4). However, this assumption has yet to be confirmed and there is a need for more biochemical characterization of decarboxylases.

In summary, this work present the biochemical characterization of two decarboxylases present in the *des* gene cluster in the genera of *Gordonia* and *Pimelobacter*. Although both decarboxylases catalyze the initial step for desferrioxamine siderophores, they showed very different properties. *Gr*DesA shows preference for L-lysine, while *Ps*DesA seems to be more promiscuous. The overall results show, that both enzymes belong to a recently discovered new type of lysine decarboxylase. Nevertheless, questions remain regarding the phylogenetic cluster formation of this type of LDCs and the close related DABA DCs and typical biochemical characteristics for the enzymes clustering together, which are worth to further investigate.

Acknowledgement

The research was founded by the Federal Ministry of Education and Research (BMBF) through the project BakSolEx (033R147) and National Science Foundation (NSF) CHE-2003658 (to P.S). DT was supported by the Federal Ministry for Innovation, Science and Research of North Rhine–Westphalia (PtJ-TRI/1411ng006)—ChemBioCat. We thank the Fulbright commission for supporting Marika Hofmann with a research scholarship for PhD students. Further we thank Keith Ray from Virginia Polytechnic Institute and State University for the cofactor analysis as well as Alvaro Gomez Baraibar and Meike Mohr from Ruhr-Universität Bochum for some activity measurements. The authors declare to have no conflict of interest.

Appendix A. Supplementary data

Supplementary data to this article can be found online at https://doi.org/10.1016/j.abb.2020.108429.

References

[1] J.B. Neilands, Microbial iron compounds, Annu. Rev. Biochem. (1981) 715–731.
[2] V. Braun, K. Hantke, Recent insights into iron import by bacteria, Curr. Opin. Chem. Biol. 15 (2011) 328–334, https://doi.org/10.1016/j.cbpa.2011.01.005.
[3] I. Schröder, E. Johnson, S. De Vries, Microbial ferric iron reductases, FEMS Microbiol. Rev. 27 (2003) 427–447, https://doi.org/10.1016/S0168-6445(03)00043-3.
[4] T.J. Brickman, M.A. McIntosh, Overexpression and purification of ferric enterobactin esterase from *Escherichia coli*. Demonstration of enzymatic hydrolysis of enterobactin and its iron complex, J. Biol. Chem. 267 (1992) 12350–12355.
[5] J.H. Crosa, C.T. Walsh, Genetics and assembly line enzymology of siderophore biosynthesis in bacteria, Microbiol. Mol. Biol. Rev. 66 (2002) 223–249, https://doi.org/10.1128/MMBR.66.2.223-249.2002.
[6] G.L. Challis, A widely distributed bacterial pathway for siderophore biosynthesis independent of nonribosomal peptide synthetases, Chembiochem 6 (2005) 601–611, https://doi.org/10.1002/cbic.200400283.
[7] D. Oves-Costales, N. Kadi, G.L. Challis, The long-overlooked enzymology of a nonribosomal peptide synthetase-independent pathway for virulence-conferring siderophore biosynthesis, Chem. Commun. (2009) 6530–6541, https://doi.org/10.1039/B913092F 0.
[8] V. de Lorenzo, A. Bindereif, B.H. Paw, J.B. Neilands, Aerobactin biosynthesis and transport genes of plasmid ColV-K30 in *Escherichia coli* K-12, J. Bacteriol. 165 (1986) 570–578.
[9] V. de Lorenzo, J.B. Neilands, Characterization of *iucA* and *iucC* genes of the aerobactin system of plasmid ColV-K30 in *Escherichia coli*, J. Bacteriol. 167 (1986) 350–355.
[10] T.J. Brickman, S.K. Armstrong, The ornithine decarboxylase gene *odc* is required for alcaligin siderophore biosynthesis in *Bordetella* spp.: putrescine is a precursor of alcaligin, J. Bacteriol. 178 (1996) 54–60, https://doi.org/10.1128/jb.178.1.54-60.1996.
[11] D. Lynch, J. O'Brien, T. Welch, P. Clarke, P. ÓCuív, J.H. Crosa, M. O'Connell, Genetic organization of the region encoding regulation, biosynthesis, and transport of rhizobactin 1021, a siderophore produced by *Sinorhizobium meliloti*, J. Bacteriol. 183 (2001) 2576–2585, https://doi.org/10.1128/JB.183.8.2576-2585.2001.
[12] M. Münzinger, H. Budzikiewicz, D. Expert, C. Enard, J.-M. Meyer, Achromobactin, a new citrate siderophore of *Erwinia chrysanthemi*, Z. Naturforsch., C: Biosci. 55 (2014) 328–332, https://doi.org/10.1515/znc-2000-5-605.
[13] G. Winkelmann, D.G. Schmid, G. Nicholson, G. Jung, D.J. Colquhoun, Bisucaberin – a dihydroxamate siderophore isolated from *Vibrio salmonicida*, an important pathogen of farmed Atlantic salmon (*Salmo salar*), Biometals Int. J. Role Met. Ions Biol. Biochem. Med. 15 (2002) 153–160.
[14] T. Tanabe, T. Funahashi, H. Nakao, S.-I. Miyoshi, S. Shinoda, S. Yamamoto, Identification and characterization of genes required for biosynthesis and transport of the siderophore Vibrioferrin in *Vibrio parahaemolyticus*, J. Bacteriol. 185 (2003) 6938–6949, https://doi.org/10.1128/JB.185.23.6938-6949.2003.
[15] F. Barona-Gómez, U. Wong, A.E. Giannakopulos, P.J. Derrick, G.L. Challis, Identification of a cluster of genes that directs desferrioxamine biosynthesis in *Streptomyces coelicolor* M145, J. Am. Chem. Soc. 126 (2004) 16282–16283, https://doi.org/10.1021/ja045774k.
[16] C.Z. Soe, A.A.H. Pakchung, R. Codd, Directing the biosynthesis of putrebactin or desferrioxamine B in *Shewanella putrefaciens* through the upstream inhibition of ornithine decarboxylase, Chem. Biodivers. 9 (2012) 1880–1890, https://doi.org/10.1002/cbdv.201200014.
[17] M.E. Tolmasky, L.A. Actis, J.H. Crosa, A histidine decarboxylase gene encoded by the *Vibrio anguillarum* plasmid pJM1 is essential for virulence: histamine is a precursor in the biosynthesis of anguibactin, Mol. Microbiol. 15 (1995) 87–95, https://doi.org/10.1111/j.1365-2958.1995.tb02223.x.
[18] Y. Li, Q. Ma, Iron acquisition strategies of Vibrio anguillarum, Front. Cell. Infect. Microbiol. 7 (2017), https://doi.org/10.3389/fcimb.2017.00342.
[19] C.E. Barancin, J.C. Smoot, R.H. Findlay, L.A. Actis, Plasmid-mediated histamine biosynthesis in the bacterial fish PathogenVibrio anguillarum, Plasmid 39 (1998) 235–244, https://doi.org/10.1006/plas.1998.1345.
[20] M. Burrell, C.C. Hanfrey, L.N. Kinch, K.A. Elliott, A.J. Michael, Evolution of a novel lysine decarboxylase in siderophore biosynthesis, Mol. Microbiol. 86 (2012) 485–499.
[21] P. Cruz-Morales, H.E. Ramos-Aboites, C. Licona-Cassani, N. Selem-Mójica, P.M. Mejía-Ponce, V. Souza-Saldívar, F. Barona-Gómez, Actinobacteria phylogenomics, selective isolation from an iron oligotrophic environment and siderophore functional characterization, unveil new desferrioxamine traits, FEMS Microbiol. Ecol. 93 (2017), https://doi.org/10.1093/femsec/fix086.
[22] T. Schupp, U. Waldmeier, M. Divers, Biosynthesis of desferrioxamine B in *Streptomyces pilosus*: evidence for the involvement of lysine decarboxylase, FEMS Microbiol. Lett. 42 (1987) 135–139, https://doi.org/10.1111/j.1574-6968.1987.tb02060.x.
[23] T. Schupp, C. Toupet, M. Divers, Cloning and expression of two genes of *Streptomyces pilosus* involved in the biosynthesis of the siderophore desferrioxamine B, Gene 64 (1988) 179–188, https://doi.org/10.1016/0378-1119(88)90333-2.
[24] F.B. Simpson, J.B. Neilands, Siderochromes in cyanophyceae: isolation and characterization of schizokinen from *Anabaena* sp, J. Phycol. 12 (1976) 44–48, https://doi.org/10.1111/j.1529-8817.1976.tb02824.x.
[25] H. Ikai, S. Yamamoto, Sequence analysis of the gene encoding a novel l-2,4-diaminobutyrate decarboxylase of *Acinetobacter baumannii*: similarity to the group II amino acid decarboxylases, Arch. Microbiol. 166 (1996) 128–131, https://doi.org/10.1007/s002030050366.
[26] H. Ikai, S. Yamamoto, Two genes involved in the 1,3-diaminopropane production pathway in *Haemophilus influenzae*, Biol. Pharm. Bull. 21 (1998) 170–173.
[27] S. Yamamoto, N. Mutoh, H. Ikai, M. Nagasaka, Occurrence of a novel L-2, 4-diaminobutyrate decarboxylase activity in some species of enterobacteriaceae, and purification and characterization of the enzymes of *Enterobacter aerogenes* and *Serratia marcescens*, Biol. Pharm. Bull. 19 (1996) 1298–1303, https://doi.org/10.1248/bpb.19.1298.
[28] M. Mehnert, G. Retamal-Morales, R. Schwabe, S. Vater, T. Heine, G.J. Levicán, M. Schlömann, D. Tischler, Revisiting the chrome azurol S assay for various metal ions, Solid State Phenom. 262 (2017) 509–512 https://doi.org/10.4028/www.scientific.net/SSP.262.509.
[29] R. Schwabe, C. Senges, J. Bandow, T. Heine, H. Lehmann, M. Schlömann, G. Levicán, D. Tischler, Cultivation dependent formation of siderophores by Gordonia rubriperticta CWB2, Microbiol. Res. 238 (2020) 126481.
[30] A. Müller, H. Zähner, Stoffwechselprodukte von Mikroorganismen: ferrioxamine aus Eubacteriales, Arch. Microbiol. 62 (1968) 257–263.
[31] V.H. Tierrafría, H.E. Ramos-Aboites, G. Gosset, F. Barona-Gómez, Disruption of the siderophore-binding *desE* receptor gene in *Streptomyces coelicolor* A3(2) results in impaired growth in spite of multiple iron–siderophore transport systems, Microb. Biotechnol. 4 (2011) 275–285, https://doi.org/10.1111/j.1751-7915.2010.00240.x.
[32] M. Mehnert, T. Heine, P. Sobrado, D. Tischler, Indentification of a gene cluster involved in desferrioxamine biosynthesis in *Gordonia rubriperincta* and *Pimelobacter simplex*, Explor. Microorg. Recent Adv. Appl. Microbiol. Brown Walker Press - Universal Publishers Inc, 2018, pp. 31–34.
[33] C.O. Esuola, O.O. Babalola, T. Heine, R. Schwabe, M. Schlömann, D. Tischler, Identification and characterization of a FAD-dependent putrescine N-hydroxylase (GorA) from *Gordonia rubripertincta* CWB2, J. Mol. Catal. B Enzym. 134 (2016) 378–389, https://doi.org/10.1016/j.molcatb.2016.08.003.
[34] M. Oelschlägel, C. Heiland, M. Schlömann, D. Tischler, Production of a recombinant membrane protein in an Escherichia coli strain for the whole cell biosynthesis of

phenylacetic acids, Biotechnol. Rep. 7 (2015) 38–43, https://doi.org/10.1016/j.btre.2015.05.002.
[35] P.G. Blommel, P.A. Martin, R.L. Wrobel, E. Steffen, B.G. Fox, High efficiency single step production of expression plasmids from cDNA clones using the Flexi Vector cloning system, Protein Expr, Purif 47 (2006) 562–570, https://doi.org/10.1016/j.pep.2005.11.007.
[36] F.W. Studier, Protein production by auto-induction in high density shaking cultures, Protein Expr, Purif 41 (2005) 207–234.
[37] C. Binda, R.M. Robinson, J.S. Martin del Campo, N.D. Keul, P.J. Rodriguez, H.H. Robinson, A. Mattevi, P. Sobrado, An unprecedented NADPH domain conformation in lysine monooxygenase NbtG provides insights into uncoupling of oxygen consumption from substrate hydroxylation, J. Biol. Chem. 290 (2015) 12676–12688, https://doi.org/10.1074/jbc.M114.629485.
[38] T.T. Ngo, K.L. Brillhart, R.H. Davis, R.C. Wong, J.H. Bovaird, J.J. Digangi, J.L. Ristow, J.L. Marsh, A.P. Phan, H.M. Lenhoff, Spectrophotometric assay for ornithine decarboxylase, Anal. Biochem. 160 (1987) 290–293.
[39] M.-E. Legaz, B. Fontaniella, R. de Armas, C. Vicente, Determination by high performance liquid chromatography of ornithine and lysine decaboxylases in sugar cane juices, Chromatographia 53 (2001) 260–265.
[40] C.M. Metzler, D.E. Metzler, Quantitative description of absorption spectra of a pyridoxal phosphate-dependent enzyme using lognormal distribution curves, Anal. Biochem. 166 (1987) 313–327, https://doi.org/10.1016/0003-2697(87)90580-X.
[41] S.C. Andrews, A.K. Robinson, F. Rodríguez-Quiñones, Bacterial iron homeostasis, FEMS Microbiol. Rev. 27 (2003) 215–237.
[42] T.C. Johnstone, E.M. Nolan, Beyond iron: non-classical biological functions of bacterial siderophores, Dalton Trans. 44 (2015) 6320–6339, https://doi.org/10.1039/C4DT03559C.
[43] M. Miethke, M.A. Marahiel, Siderophore-based iron acquisition and pathogen control, Microbiol. Mol. Biol. Rev. 71 (2007) 413–451, https://doi.org/10.1128/MMBR.00012-07.
[44] A.D. Berti, M.G. Thomas, Analysis of achromobactin biosynthesis by Pseudomonas syringae pv. syringae B728a, J. Bacteriol. 191 (2009) 4594–4604, https://doi.org/10.1128/JB.00457-09.
[45] S. Schmelz, N. Kadi, S.A. McMahon, L. Song, D. Oves-Costales, M. Oke, H. Liu, K.A. Johnson, L.G. Carter, C.H. Botting, M.F. White, G.L. Challis, J.H. Naismith, AcsD catalyzes enantioselective citrate desymmetrization in siderophore biosynthesis, Nat. Chem. Biol. 5 (2009) 174–182, https://doi.org/10.1038/nchembio.145.
[46] T.A. Keating, C.G. Marshall, C.T. Walsh, Vibriobactin biosynthesis in *Vibrio cholerae* : VibH is an amide synthase homologous to nonribosomal peptide synthetase condensation domains †, Biochemistry 39 (2000) 15513–15521, https://doi.org/10.1021/bi001651a.
[47] D.R. Morris, R.H. Fillingame, Regulation of amino acid decarboxylation, Annu. Rev. Biochem. 43 (1974) 303–321, https://doi.org/10.1146/annurev.bi.43.070174.001511.